

Diamagnetic drift effects on the low- n magnetohydrodynamic modes at the high mode pedestal with plasma rotation

L. J. Zheng, M. T. Kotschenreuther, and P. Valanju

Institute for Fusion Studies, University of Texas at Austin, Austin, TX 78712

(Dated: March 11, 2014)

Abstract

The diamagnetic drift effects on the low- n magnetohydrodynamic instabilities at the high-mode (H-mode) pedestal are investigated in this paper with the inclusion of bootstrap current for equilibrium and rotation effects for stability, where n is the toroidal mode number. The AEGIS (Adaptive EiGenfunction Independent Solutions) code [L. J. Zheng, M. T. Kotschenreuther, J. Comp. Phys. **211**, (2006)] is extended to include the diamagnetic drift effects. This can be viewed as the lowest order approximation of the finite Larmor radius effects in consideration of the pressure gradient steepness at the pedestal. The H-mode discharges at Jointed European Torus (JET) is reconstructed numerically using the VMEC code [P. Hirshman and J. C. Whitson, Phys. Fluids **26**, 3553 (1983)], with bootstrap current taken into account. Generally speaking, the diamagnetic drift effects are stabilizing. Our results show that the effectiveness of diamagnetic stabilization depends sensitively on the safe factor value (q_s) at the safety-factor reversal or plateau region. The diamagnetic stabilization are weaker, when q_s is larger than an integer; while stronger, when q_s is smaller or less larger than an integer. We also find that the diamagnetic drift effects also depend sensitively on the rotation direction. The diamagnetic stabilization in the co-rotation case is stronger than in the counter rotation case with respect to the ion diamagnetic drift direction.

PACS numbers: 52.35.Py, 52.55.Fa, 52.55.Hc

I. INTRODUCTION

The high mode (H-mode) confinement¹ has today been adopted as a reference for next generation tokamaks, especially for ITER. However, the H-mode confinement is often tied with the damaging edge localized modes (ELMs).¹ ELMs can potentially damage divertor plates, due to the heat load they cause. This is particularly a challenging issue for a big devices like ITER. Therefore, the investigation for how to mitigate ELMs at the H-mode discharges is important. While various solutions are proposed, an interesting solution is to develop the so-called quiescent H-mode (QH-mode).² ELMs are avoided in the QH-modes, due to the excitation of the so-called edge harmonic oscillations (EHOs) or outer modes (OMs),^{2,3} that pump out plasma energy in a mild way without exciting the damaging ELMs.

The current paper is aimed at further understanding of ELMs and EHOs in the H-mode or QH-mode discharges. In particular, we investigate the diamagnetic drift effects on low- n ($n = 1, 2$, and 3) magnetohydrodynamic (MHD) instabilities at the H-mode pedestal with the inclusion of bootstrap current for equilibrium and rotation effects for stability, where n is toroidal mode number. Note that, when bootstrap current is taken into account, a safety-factor reversal or plateau can be generated at the pedestal.⁴ We have shown that the modes of infernal type (or fat interchange modes)^{5,6} can prevail at the safety-factor reversal or plateau region and found that such a type of modes has the typical EHO features at QH-mode discharges.^{7,8} There is a physical ground for us to extend these investigations to include the diamagnetic drift effects. We note that the ion diamagnetic frequency (ω_{*i}) is directly proportional to pressure gradient and inversely proportional to density. This leads the ion diamagnetic frequency ω_{*i} to become big and vary dramatically at the pedestal, where the infernal modes tend to develop. Therefore, the current investigation of diamagnetic drift effects is interesting.

We point out that the peeling or kink/peeling modes were previously proposed to explain EHOs or OMs. The diamagnetic stabilization effects on the peeling, ballooning, and peeling-ballooning modes have been studied in Refs. 9–12. In difference from these investigations we include the bootstrap current effects on the equilibrium. This inclusion leads the safety factor profile to change⁴ and subsequently the MHD modes to behave differently. In our earlier works^{7,8} we prove that the MHD modes of infernal mode type^{5,6} can prevail in this case. The diamagnetic stabilization effects on the infernal modes also are different,

as compared those reviewed in Ref. 12. Based on the ballooning mode investigation,¹⁰ Reference 12 concludes that, when there is a radial variation in the diamagnetic frequency ω_{*i} , the diamagnetic stabilization is less effective. Instead, we find that, when the bootstrap current effect on the equilibrium is taken into account, the diamagnetic stabilization can be effective, depending sensitively on the safety factor value at the region where the safety factor is flat or reversed and also on the toroidal rotation direction. Besides, we point out that the current investigation is based on the two dimensional free boundary AEGIS (Adaptive EiGenfunction Independent Solutions) code,¹³ while the previous conclusion about the ineffectiveness of the diamagnetic stabilization is based on the conventional one dimensional ballooning representation.^{10,12} As pointed out in Ref. 14 the conventional ballooning mode representation cannot be used at the plasma edge. Therefore, the current investigation extends the existing investigations based on the peeling-ballooning mode formalism.

This paper is arranged as follows: In Sec. II the numerical schemes for equilibrium and stability analyses are given; In Sec. III the numerical results are presented; Conclusions and discussion are given in the last section.

II. NUMERICAL SCHEME

In this section we describe the numerical scheme for equilibrium and stability studies. For equilibrium we focus our investigation on the JET-like QH-mode discharges. The plasma cross section is shown in Fig. 1. The conformal wall is used in our calculations. Furthermore, we consider only the subsonic rotation case, i.e., the rotation frequency is assumed to be much lower than the ion acoustic frequency. In this case the rotational effects of centrifugal force and Coriolis force both on equilibrium and stability can be neglected.^{15,16} We then include the rotational effects only through a Doppler frequency shift in the stability analysis.

To study the QH mode, we consider the low collisionality regime. In this regime the steep pressure gradient at the pedestal region can induce a strong bootstrap current. As in Refs. 7 and 8 we use the STELLOPT¹⁷ code (part of the VMEC¹⁸ code suite) to compute the collisionless limit of the bootstrap current.¹⁹ For parameters typical of QH mode pedestals with normalized collision frequency $\nu^* = 0.05$ and inverse aspect ratio $r/R = 0.3$, the bootstrap current is approximately 80%-90% of the collisionless limit.²⁰ In addition, numerical calculations find that there are modest modifications due to finite poloidal gyroradius²⁰ (which

have yet to be evaluated for QH modes). Our equilibrium results are consistent to the previous calculations with other codes as given in Ref. 4. Taking into account the bootstrap current in the equilibrium calculation, we found that a safety-factor (q) reversal or plateau can indeed appear in the pedestal region. We denote the safety factor value at the region where the safety factor is flat or reversed as q_s .

Our physics intuition leads to examine the difference between the cases with q_s larger and smaller than an integer number. The equilibria are therefore constructed to have different q_s , while minimizing other profile changes. The q profile change is resulted from the change of toroidal current. Subsequently, the pressure profile is scaled up or down to keep beta normal constant. We use five different equilibria for stability analyses as mostly used in Refs. 7 and 8, with the safety factor at the plateau, q_s , ranging from 4.2, 4.1, 4.05, 4, and 3.96. The safety factor and toroidal current profiles are plotted in Fig. 2; while the corresponding pressure profiles are plotted in Fig. 3. We keep the beta normal the same in the five equilibria by scaling the overall pressure profile appropriately.

As one can imagine, the appearance of safety factor plateau can minimize the magnetic shear stabilization and cause the “fat interchange modes” (i.e., infernal modes) to develop locally.^{7,8} We consider only the low- n modes: $n = 1, 2$, and 3. The MHD instabilities in this type of equilibria are investigated numerically using the AEGIS code,¹³ with both the diamagnetic and apparent mass effects taken into account. In including the diamagnetic drift effects we use the frequency modification: $(\omega + n\Omega)^2 \rightarrow \hat{\omega}^2 \equiv (\omega + n\Omega)(\omega + n\Omega - \omega_{*i})$, where ω is the mode frequency and Ω is the toroidal rotation frequency. This modification can be viewed as keeping the finite Larmor radius effects in lowest order in consideration of the pressure gradient steepness at the pedestal.^{21,22} The adaptive numerical scheme of AEGIS code allows us to study the rotation-induced continuum damping.²³

The basic MHD equation used for our stability analyses is as follows:

$$-\rho_m \hat{\omega}^2 \boldsymbol{\xi} = \delta \mathbf{J} \times \mathbf{B} + \mathbf{J} \times \delta \mathbf{B} - \nabla \delta P,$$

where $\boldsymbol{\xi}$ is the perpendicular field line displacement, \mathbf{B} denotes the equilibrium magnetic field, $\delta \mathbf{B} = \nabla \times \boldsymbol{\xi} \times \mathbf{B}$ is the perturbed magnetic field, \mathbf{J} represents the equilibrium current density, $\mu_0 \delta \mathbf{J} = \nabla \times \delta \mathbf{B}$ is the perturbed current density, μ_0 is the magnetic constant, P represents the equilibrium pressure, $\delta P = -\boldsymbol{\xi} \cdot \nabla P$ is the perturbed pressure of convective part, and the perturbed quantities are tagged with δ except $\boldsymbol{\xi}$. The plasma compressibility

effect does not appear in this equation explicitly. Since the mode frequencies we are studying are much smaller than the ion acoustic wave frequency, the plasma compressibility results only in the so-called apparent mass effect, as proved in Ref. 24. Therefore, we include the plasma compressibility effect by regarding ρ_m as the total mass, i.e., the sum of perpendicular mass and parallel mass (i.e., the apparent mass in the perpendicular momentum equation) according to Ref. 24.

Note that the EHOs (or OMs) observed experimentally have finite frequencies, about 10 kHz for $n = 1$ modes,^{2,3} which is much larger than the wall magnetic diffusion time. For modes with such high frequencies the wall behaves as a perfect conductor. Therefore, our calculations focus only on the perfectly conducting wall case. As in Ref. 7 we use the combined methods of the Nyquist diagram and the analytic continuation of the dispersion relation to determine the unstable roots.

III. NUMERICAL RESULTS

The diamagnetic drift effects on peeling-ballooning modes have been discussed in Ref. 12. The discussion is based on the earlier research about diamagnetic stabilization effects on the ballooning modes in Ref. 10. When the bootstrap current effects on the equilibrium are taken into account, however, the infernal mode appears and its behavior deviates from that of ballooning modes. Consequently, one can expect the diamagnetic drift effects to behave quite differently. To show these different features we mainly investigate five equilibria with safety factor at the plateau, q_s , ranging from 4.2, 4.1, 4.05, 4, and 3.96. From Figs. 2 and 3 one can see that, besides the change in q_s , these five equilibria are almost identical. However, as shown in the following numerical results, the diamagnetic stabilization effects on these equilibria are vastly different. In our investigation, the rotation frequency profile is assumed to be the same as the pressure profile and the density profile is assumed to be the same as the temperature one.

First, we point out that the diamagnetic drift effects are generally stabilizing for infernal modes, as one may expect. But, the effectiveness of diamagnetic stabilization depends on the safety factor value at the plateau. Figures 5 and 6 show the eigen frequencies and growth rates of $n = 1$ modes versus the wall position respectively for the cases without and with the diamagnetic drift effects. The frequencies are normalized by the Alfvén frequency

at the magnetic axis and the wall position is normalized by the minor radius in the mid-plane in this work. We have assumed the direction of rotation is the same as the direction of ion diamagnetic drift motion in most of the investigations in this work, unless it is indicated otherwise. In these figures the rotation frequency at the magnetic axis is $\Omega = 0.03$ and the safety factor value (q_s) at the safety-factor reversal or plateau region is used as a parameter. The typical real and imaginary eigen functions of $n = 1$ modes for the case without the diamagnetic drift effects are shown respectively in Figs. 7a and 7b and those for the case with the diamagnetic drift effects are shown respectively in Figs. 8a and 8b. From Figs. 7 and 8 one can see that the $m/n = 4/1$ harmonic, which is resonant at the safety factor plateau, appears bigger and broad as compared to the usual kink modes. Their features as the infernal modes have been discussed in Refs. 7 and 8. Here, we concentrate on discussing the diamagnetic drift effects. From Figs. 5 and 6 one can see that the growth rates with the diamagnetic drift effects are generally smaller than those without the diamagnetic drift effects. This shows the general stabilization of the diamagnetic drift effects. Bigger frequencies in the case with the diamagnetic drift effects as compared to the cases without the diamagnetic drift effects are because the rotation is assumed to be in the ion diamagnetic drift direction in Fig. 6. From Fig. 6 one can also see that the smaller q_s case has a larger frequency. This is because, when q_s reduces, the $m = 4$ infernal harmonic moves outwardly from the pedestal top and consequently the amplitude of the diamagnetic frequency increases (see the ω_{*i} profile in Fig. 4). Notably, our results show that the diamagnetic drift effects depend sensitively on the q_s value. The diamagnetic drift effects are weaker, when q_s is far larger than an integer (here, it is “4”); while stronger, when q_s is less larger or smaller than an integer. This can be seen from Fig. 6. In Fig. 6 the growth rate for $q_s = 4.2$ case is one order larger than the $q_s = 4.1$ case. The modes are stable when $q_s = 4.0$ and 3.96. We also check the further lower q_s case, for example $q_s = 3.92$. A full diamagnetic stabilization is found as well. This can be explained by inspecting the profile of ion diamagnetic drift frequency ω_{*i} in Fig. 4 together with the $m/n = 4/1$ infernal harmonic accumulating point. When q_s is far larger than an integer “4”, the $m = 4$ infernal harmonic tends to accumulate at the inner side of the safety-factor reversal or plateau region. Noting that the ion diamagnetic drift frequency ω_{*i} is smaller in this region, one can expect a weaker diamagnetic stabilization to result. Whereas, when q_s is less larger than an integer or even smaller than an integer, the accumulation point of the infernal harmonic moves outwardly relative to the pedestal top.

Noting that the ion diamagnetic drift frequency ω_{*i} becomes larger in this region, one can understand why a stronger diamagnetic stabilization should result.

We also explore the diamagnetic drift effects for various rotation speeds. Figures 9 and 10 show the eigen frequencies and growthrates of $n = 1$ modes versus the rotation frequency at the magnetic axis respectively for the cases without and with the diamagnetic drift effects. They are for the equilibrium with $q_s = 4.2$. It is interesting to point out that the frequency difference between the cases with and without the diamagnetic drift effects remains about the same, as the rotation frequency varies. The difference is about 0.003. The formula $(\omega + n\Omega)(\omega + n\Omega - \omega_{*i}) = (\omega + n\Omega - \omega_{*i}/2)^2 - \omega_{*i}^2/4$ tells that the ω_{*i} induced frequency shift is $\omega_{*i}/2$. From the ω_{*i} profile in Fig. 4 and the eigen mode plots in Fig. 8 one can see that the location for $\omega_{*i}/2 = 0.003$ is around where the $m = 4$ Fourier harmonic of infernal mode type locates. This again confirms the infernal mode feature of the instabilities.

The rotation direction effects are investigated as well and the results are shown in Fig. 11. In this figure $q_s = 4.1$ and the diamagnetic stabilization effects are taken into account. Without the diamagnetic stabilization effects the mode growthrate remains unchanged and only the mode frequency changes signs, as the rotation direction switches. When the diamagnetic stabilization effects are taken into consideration, Figure 10 shows that the frequency difference for two rotation directions is about 0.006. Similar to the discussion for Figs. 9 and 10 in the previous paragraph, this again shows that the ω_{*i} value at where the $m = 4$ Fourier harmonic locates plays a key role — an infernal mode feature. Figure 11 shows that the stabilization effects for co-rotation case is much stronger than for counter-rotation case with respect to the ion diamagnetic drift direction. As an infernal mode feature, the mode frequency tends to match the local sum of rotation and diamagnetic frequencies for $m = 4$ infernal harmonic. However, in the toroidal geometry the sideband effects have to be considered as well. Note that rotation and diamagnetic frequencies have radial profiles. The combined effects of rotation and diamagnetic frequencies on the sidebands between the co-rotation and counter-rotation cases are different. A larger sum of rotation and diamagnetic frequencies gives rise to a stronger continuum damping effects.²³ This leads to the counter-rotation case becomes more unstable than the co-rotation case as shown in Fig. 11.

We have discussed the $n = 1$ modes above. Now, we turn to the $n = 2$ and 3 modes. Figure 12 gives the dependence of mode frequencies and growthrates for $n = 1 - 3$ modes on the wall position without the diamagnetic drift effects and Fig. 13 gives the dependence

of mode frequencies and growth rates for $n = 1$ and 2 modes on the wall position with the diamagnetic drift effects. Both figures are related to the $q_s = 4.2$ equilibrium and rotation frequency at the magnetic axis is $\Omega = 0.03$. As pointed out in Ref. 8 without the diamagnetic drift effects Fig. 12 shows that the mode frequencies follows the frequency-multiplying rule: $\omega = n\Omega_s$ for $n = 1 - 3$ modes, where Ω_s is about the rotation frequency at the pedestal top. With the diamagnetic drift effects being taken into account we found that the frequency-multiplying rule $\omega = n\Omega_s$ are still roughly kept for $n = 1$ and 2 modes. The $n = 3$ modes, however, do not appear in Fig. 13, since they are stabilized in this equilibrium. Nevertheless, we note that in the nonlinear case the $n = 1$ and 2 modes can couple to give rise to the $n = 3$ modes with frequency being the sum of $n = 1$ and 2 mode frequencies. In view of this the frequency-multiplying rule can still be expected for low- n modes with the diamagnetic drift effects taken into account in the nonlinear description. We also point out that in the $n = 3$ case (or even $n = 2$ case) other kinetic effects may need to be considered, since the diamagnetic drift frequency for $n = 3$ is larger.

IV. CONCLUSIONS AND DISCUSSION

The diamagnetic drift effects on the low- n magnetohydrodynamic instabilities at the high-mode (H-mode) pedestal are investigated in this paper. In view of the steep pressure gradient in the pedestal region, the inclusion of diamagnetic drift effects can be regarded as the inclusion of finite Larmor radius effects in the lowest order.^{21,22} We focus our investigation on the JET-like QH-mode discharges. Subsonic plasma rotation effects are included in the investigation, especially the induced continuum damping effect. The differences of current studies from the previous ones based on the ballooning or peeling-ballooning pictures in Refs. 10. and 12 mainly lie in the following aspects: First, we include the bootstrap current effects on the equilibrium so that a safety factor plateau is resulted at the pedestal region. Because of that our focus is shifted to the diamagnetic drift effects on the $m/n = 4/1$ infernal harmonic. Second, the current calculation is based on the two dimensional free boundary MHD code: AEGIS, while the researches in Ref. 12 is based on the conventional one dimensional ballooning representation. Because of these differences our research yields several interesting new results, which have not been reported in the previous studies.

First, we note that the diamagnetic frequency (ω_{*i}) is directly proportional to pressure

gradient and inversely proportional to density. This leads the diamagnetic frequency ω_{*i} to become big and vary dramatically at the pedestal, where the infernal modes tend to develop. In view of this fact we find that the diamagnetic drift effects depend sensitively on the safety factor value (q_s) at the safety-factor reversal or plateau region. The diamagnetic stabilization effects are weaker, when q_s is larger than an integer; while stronger, when q_s is smaller or less larger than an integer. This is because, when q_s is far larger than an integer, the infernal modes tends to accumulate at the inner side of the safety-factor reversal or plateau region, where ω_{*i} is smaller, while when q_s is smaller or less than an integer the infernal modes tends to move outwardly from the pedestal top, where ω_{*i} becomes larger. A larger diamagnetic frequency amplitude ω_{*i} at where the infernal harmonic develops gives a stronger stabilization effects. This explains why the q_s value is so critical.

We also find that the diamagnetic drift effects depend sensitively on the rotation direction. Counter rotation results in a weak diamagnetic stabilization, while co-rotation gives rise to a strong diamagnetic stabilization with respect to the ion diamagnetic drift direction. The reason is as follows. The co-rotation results in a larger sum of rotation and diamagnetic frequencies. Consequently, it leads a stronger continuum damping especially from the sidebands.

We have studied the $n = 2$ and 3 modes as well. We find that the $n = 3$ modes tends to be stabilized by the diamagnetic drift effects for the equilibria we considered, because the diamagnetic stabilization effects is proportional to $\omega_{*i}^2/4$ and ω_{*i} is directly proportional to the mode number n . With the diamagnetic drift effects being taken into account we found that the frequency-multiplying rule $\omega = n\Omega_s$ are still roughly kept for $n = 1$ and 2 modes. We discuss that the possible nonlinear coupling can lead to the frequency-multiplying rule to hold for $n = 3$ modes as well.

The current investigation is focused on the low n modes. In this case the mode frequency in the rotating frame for infernal harmonic is still low, so that the wave-particle resonance effects may be excluded. In the higher mode number case the wave-particle resonance effects need to be considered. Due to the dramatic variation of the diamagnetic frequency at the pedestal, a fully kinetic treatment is strongly preferred for this subject. The current investigation may be regarded as an extension of existing researches for diamagnetic stabilization.^{10,12} So far in this field the fully kinetic treatment of pedestal physics is still limited to using the fixed boundary ballooning mode formalism. Most of peeling ballooning

mode calculations are still based on the ideal MHD framework. Fully kinetic treatment for free boundary problems is challenging and will be considered in the future.

This research is supported by U. S. Department of Energy, Office of Fusion Energy Science.

-
- ¹ F. Wagner, G. Becker, K. Behringer, D. Campbell, A. Eberhagen, W. Engelhardt, G. Fussmann, O. Gehre, J. Gernhardt, G. V. Gierke, G. Haas, M. Huang, F. Karger, M. Keilhacker, O. Klüber, M. Kornherr, K. Lackner, G. Lisitano, G. G. Lister, H. M. Mayer, D. Meisel, E. R. Müller, H. Murmann, H. Niedermeyer, W. Poschenrieder, H. Rapp, H. Röhr, F. Schneider, G. Siller, E. Speth, A. Stäbler, K. H. Steuer, G. Venus, O. Vollmer, and Z. Yü, *Phys. Rev. Lett.* **49**, 1408 (1982).
- ² K. H. Burrell, W. P. West, E. J. Doyle, M. E. Austin, T. A. Casper, P. Gohil, C. M. Greenfield, R. J. Groebner, A. W. Hyatt, R. J. Jayakumar, D. H. Kaplan, L. L. Lao, A. W. Leonard, M. A. Makowski, G. R. McKee, T. H. Osborne, P. B. Snyder, W. M. Solomon, D. M. Thomas, T. L. Rhodes, E. J. Strait, M. R. Wade, G. Wang, and L. Zeng, *Phys. Plasmas* **12**, 056121 (2005).
- ³ E. R. Solano, P. J. Lomas, B. Alper, G. S. Xu, Y. Andrew, G. Arnoux, A. Boboc, L. Barrera, P. Belo, M. N. A. Beurskens, M. Brix, K. Crombe, E. de la Luna, S. Devaux, T. Eich, S. Gerasimov, C. Giroud, D. Harting, D. Howell, A. Huber, G. Kocsis, A. Korotkov, A. Lopez-Fraguas, M. F. F. Nave, E. Rachlew, F. Rimini, S. Saarelma, A. Sirinelli, S. D. Pinches, H. Thomsen, L. Zabeo, and D. Zarzoso, *Phys. Rev. Lett.* **104**, 185003 (2010).
- ⁴ C. E. Kessel, G. Giruzzi, A. C. C. Sips, R. V. Budny, J. F. Artaud, V. Basiuk, F. Imbeaux, E. Joffrin, M. Schneider, M. Murakami, T. Luce, Holger St John, T. Oikawa, N. Hayashi, T. Takizuka, T. Ozeki, Y.-S. Na, J. M. Park, J. Garcia, and A. A. Tucillo, *Nucl. Fusion* **47**, 1274 (2007).
- ⁵ J. Manickam, N. Pomphrey, and A. M. M. Todd, *Nucl. Fusion* **27**, 1461 (1987).
- ⁶ F. L. Waelbroeck and R. D. Hazeltine, *Phys. Fluids* **31**, 1217 (1988) .
- ⁷ L. J. Zheng, M.T. Kotschenreuther and P. Valanju, *Phys. Plasmas* **20**, 012501 (2013) .
- ⁸ L. J. Zheng, M.T. Kotschenreuther and P. Valanju, *Nucl. Fusion* **53**, 063009 (2013) .
- ⁹ L. J. Zheng, *Phys. Fluids B: Plasma Phys.* **5**, 1402 (1993) .
- ¹⁰ R. J. Hastie, Peter J. Catto, and J. J. Ramos, *Phys. Plasmas* **7**, 4561 (2000).
- ¹¹ P. B. Snyder, K. H. Burrell, H. R. Wilson, M. S. Chu, M. E. Fenstermacher, A. W. Leonard, R. A. Moyer, T. H. Osborne, M. Umansky, W. P. West, and X. Q. Xu, *Nucl. Fusion* **47**, 961 (2007).
- ¹² H. R. Wilson, S. C. Cowley, A. Kirk, and P. B. Snyder, *Plasma Phys. Control. Fusion* **48**, A71

- (2006) .
- ¹³ L.-J. Zheng and M. Kotschenreuther, J. Comp. Phys. **211**, 748 (2006) .
 - ¹⁴ L.-J. Zheng, Phys. Plasmas **19**, 102506 (2012).
 - ¹⁵ F. L. Waelbroeck and L. Chen, Phys. Fluids B: Plasma Phys. **3**, 601 (1991) .
 - ¹⁶ L.-J. Zheng, M. S. Chu, and L. Chen, Phys. Plasmas **6**, 1217 (1999) .
 - ¹⁷ D. A. Spong, S. P. Hirshman, L. A. Berry, J. F. Lyon, R. H. Fowler, D. J. Strickler, M. J. Cole, B. N. Nelson, D. E. Williamson, A. S. Ware, D. Alban, R. Snchez, G. Y. Fu, D. A. Monticello, W. H. Miner, and P. M. Valanju, Nucl. Fusion **41**, 711 (2001) .
 - ¹⁸ P. Hirshman and J. C. Whitson, Phys. Fluids **26**, 3553 (1983) .
 - ¹⁹ K. C. Shaing, E. C. Crume, J. S. Tolliver, S. P. Hirshman, and W. I. van Rij, Phys. Fluids **B1**, 148 (1989) .
 - ²⁰ M. Landreman and D. R. Ernst, Plasma Physics and controlled fusion **54** , 115006 (2012).
 - ²¹ L.-J. Zheng, Phys. Fluids B: Plasma Phys. **5**, 1962 (1993).
 - ²² L. J. Zheng, M. T. Kotschenreuther, and J. W. Van Dam, Phys. Plasmas **14**, 072505 (2007).
 - ²³ L.-J. Zheng, M. Kotschenreuther, and M. S. Chu, Phys. Rev. Lett. **95**, 255003 (2005) .
 - ²⁴ J. M. Greene and J. L. Johnson, Phys. Fluids **5**, 510 (1962).

Figure captions:

Fig. 1: The cross section of JET-like configuration. The horizontal coordinate X represents the distance from the axisymmetric axis. The vertical coordinate Y is the height from the vertical mid-plane.

Fig. 2. Safety factor (q) and parallel current density (J) profiles versus normalized poloidal magnetic flux. The safety factor values at the plateau range from 4.2, 4.1, 4.05, 4, to 3.96.

Fig. 3. Pressure profiles versus normalized poloidal magnetic flux for the cases with the safety factor values at the plateau range from 4.2, 4.1, 4.05, 4, to 3.96. Pressure is normalized by B^2/μ_0 at the magnetic axis.

Fig. 4. The diamagnetic frequency of $n = 1$ modes versus normalized poloidal magnetic flux for the case with $q_s = 4.1$. Since the pressure profiles for five cases we consider are almost identical as shown in Fig. 3, the diamagnetic frequencies for other cases resemble to this figure.

Fig. 5. Eigen frequencies and growthrates of $n = 1$ modes versus wall position for the cases with $q_s = 4.2, 4.1, 4.05$, and 4 without the diamagnetic drift effects. The four growthrate curves are below the frequency curves.

Fig. 6. Eigen frequencies and growthrates of $n = 1$ modes versus wall position for the cases with $q_s = 4.2, 4.1$, and 4.05 with diamagnetic drift effects. The cases with $q_s = 4, 3.96$, and 3.92 are stable, when the diamagnetic drift effects are taken into account. Note that the growthrate scale for the case with $q_s = 4.2$ is 10 times larger as indicated in the figure.

Fig. 7. The real (a) and imaginary (b) eigen functions of $n = 1$ modes versus normalized poloidal magnetic flux for the case with $q_p = 4.2, b = 1.5, \Omega = 0.03$, and without the diamagnetic drift effects. The q profile and the rational surfaces are also given.

Fig. 8. The real (a) and imaginary (b) eigen functions of $n = 1$ modes versus normalized poloidal magnetic flux for the case with $q_p = 4.2, b = 1.5, \Omega = 0.03$, and with the diamagnetic drift effects. The q profile and the rational surfaces are also given.

Fig. 9. Eigen frequencies and growthrates of $n = 1$ modes versus the rotation frequency at the magnetic axis for the case with $q_s = 4.2$ without diamagnetic drift effects. Wall position is used as the parameter. The three growthrate curves are below the frequency curves.

Fig. 10. Same as Fig. 9, but the diamagnetic drift effects are taken into account.

Fig. 11. Eigen frequencies and growthrates of $n = 1$ modes versus wall position for the

case with $q_s = 4.2$ with the diamagnetic drift effects being taken into account. The results with opposite rotation directions are displayed. The two growthrate curves are below the frequency curves.

Fig. 12. Eigen frequencies and growthrates of $n = 1 - 3$ modes versus wall position for the case with $q_s = 4.2$ and without the diamagnetic drift effects being taken into account. The three growthrate curves are below the frequency curves.

Fig. 13. Eigen frequencies and growthrates of $n = 1$ and 2 modes versus wall position for the case with $q_s = 4.2$ and with the diamagnetic drift effects being taken into account. The two growthrate curves are below the frequency curves.

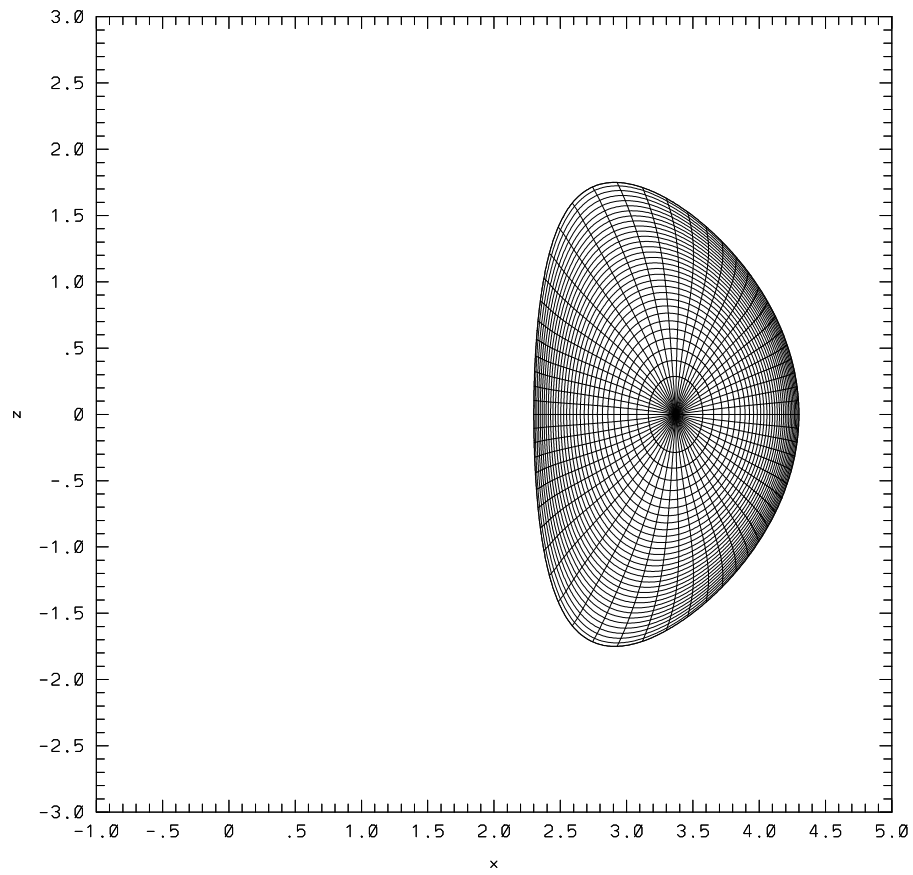


Fig. 1

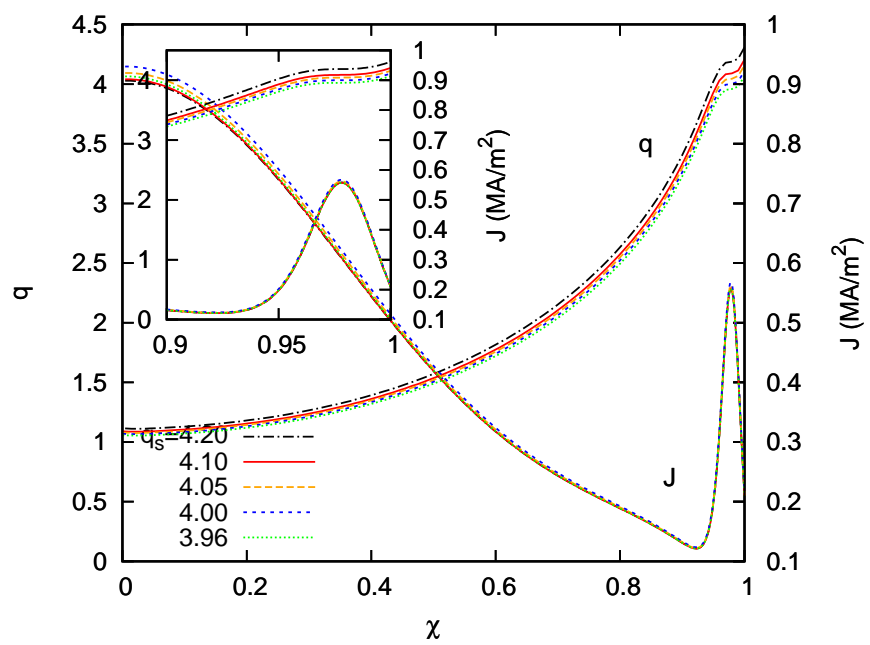


Fig. 2

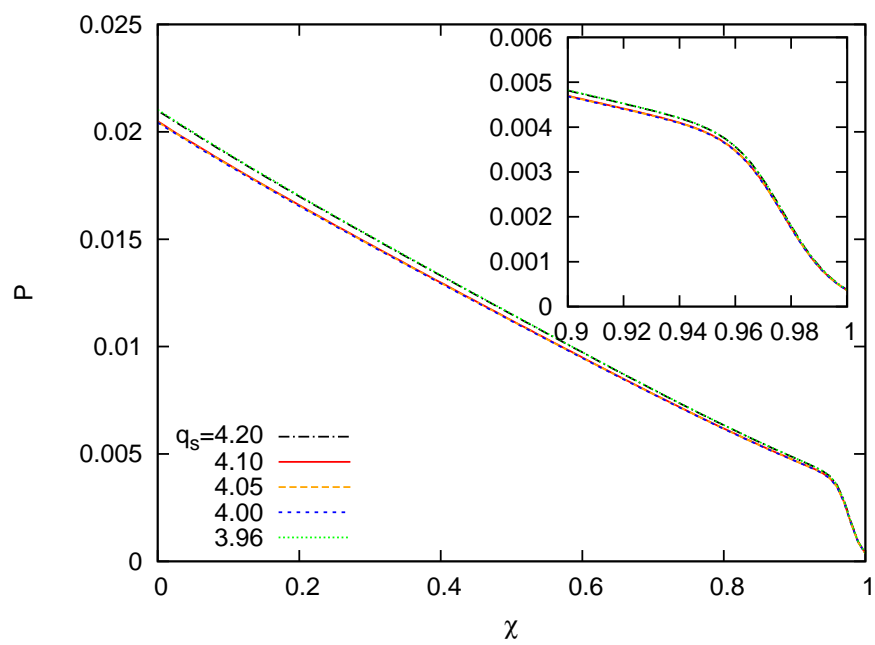


Fig. 3

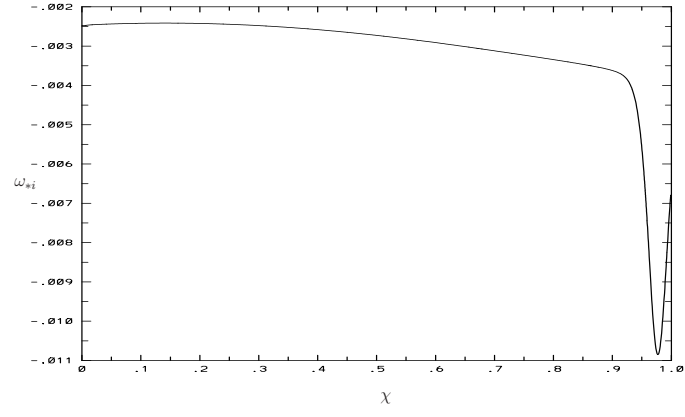


Fig. 4

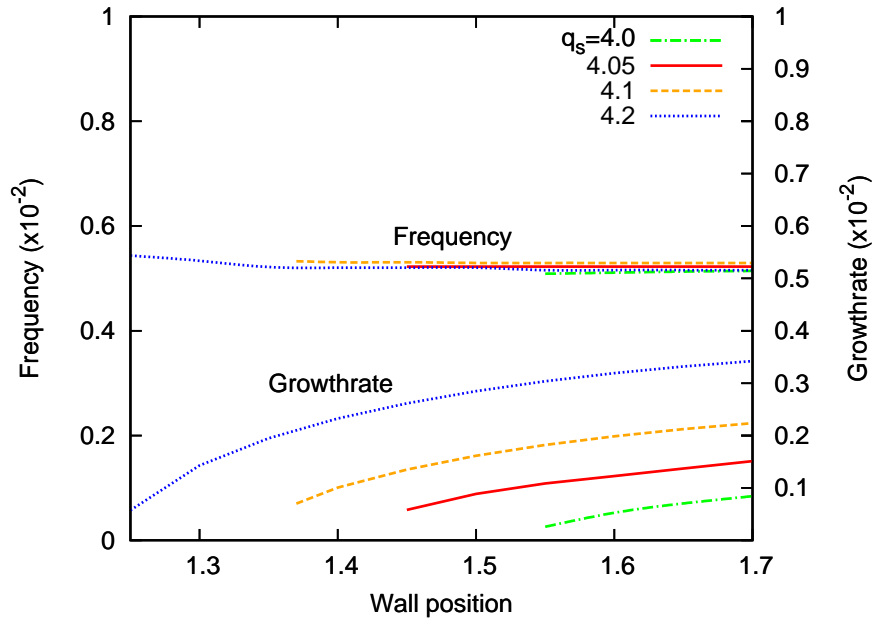


Fig. 5

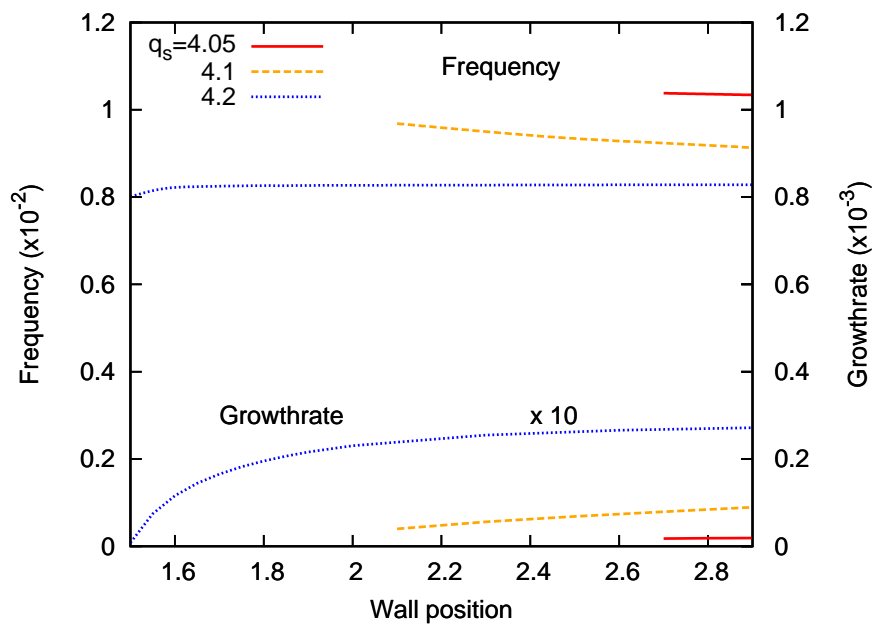


Fig. 6

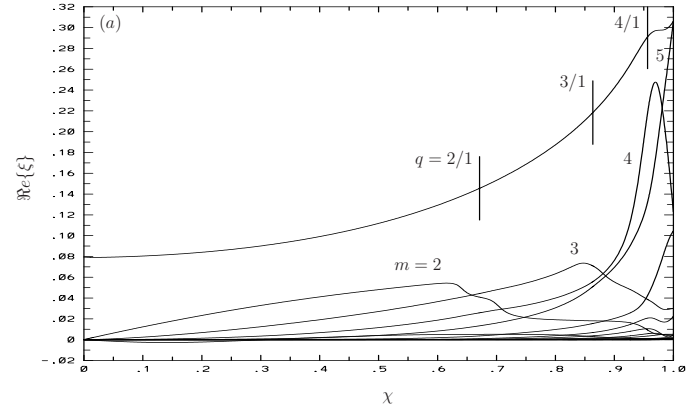


Fig. 7a

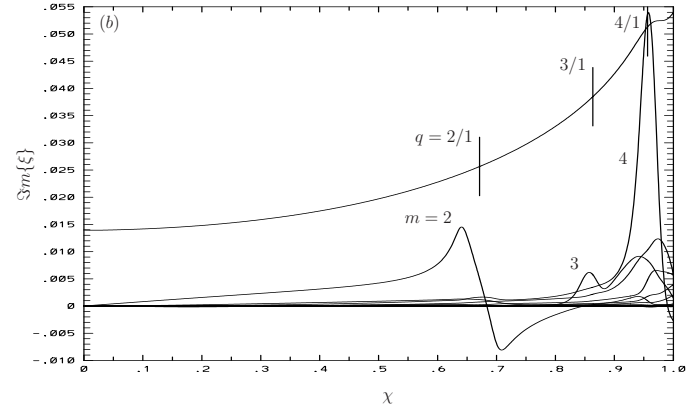


Fig. 7b

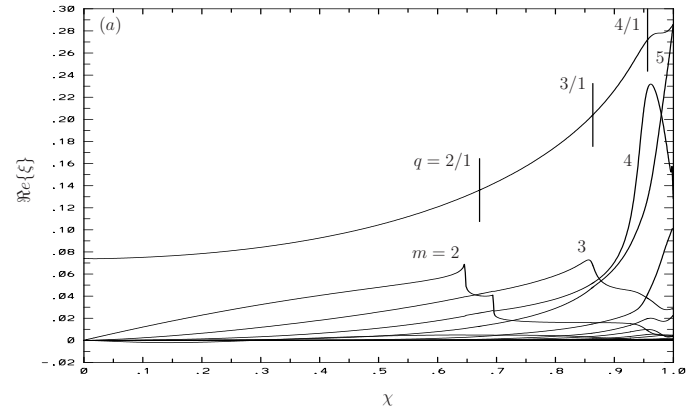


Fig. 8a

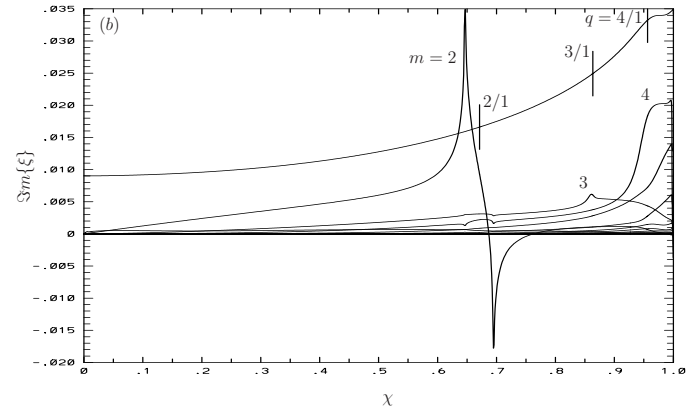


Fig. 8b

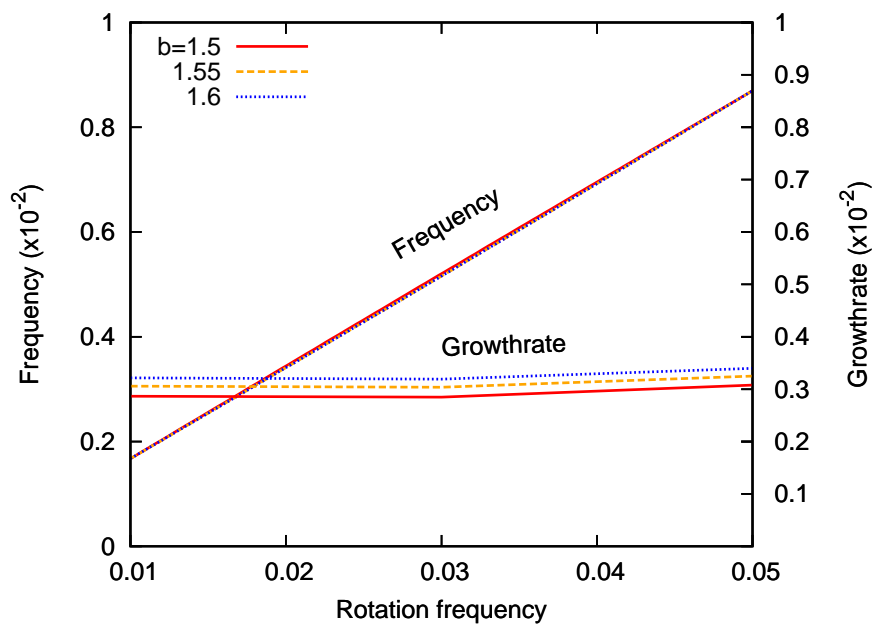


Fig. 9

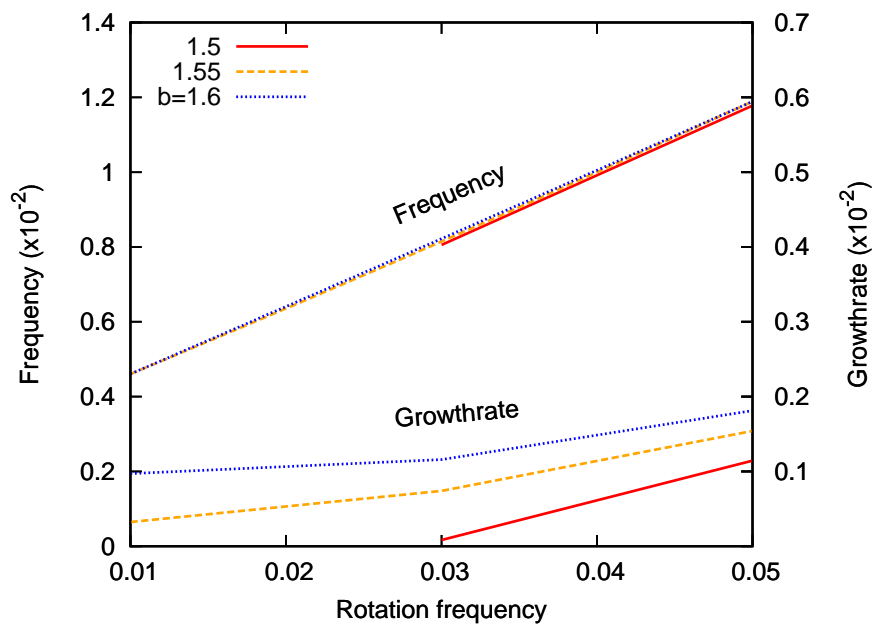


Fig. 10

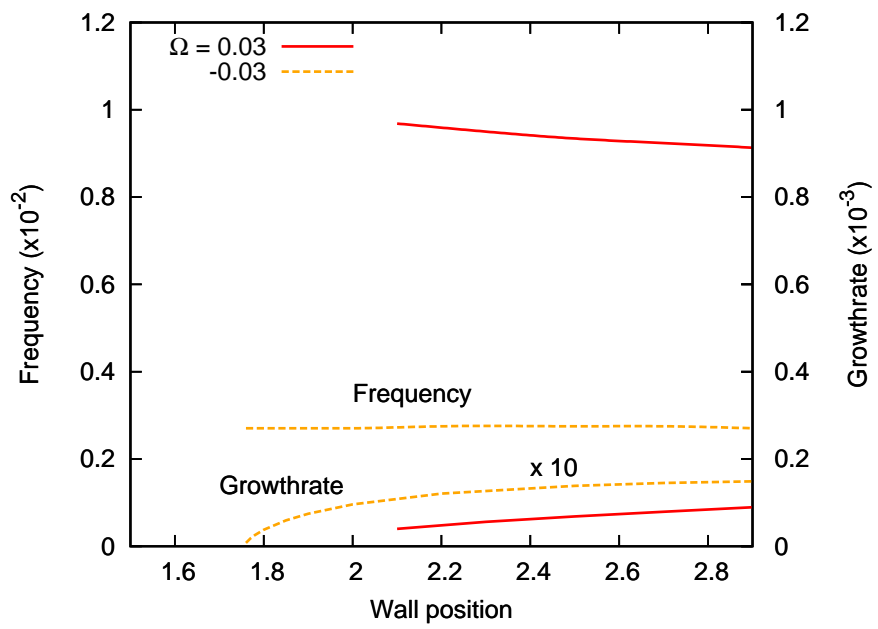


Fig. 11

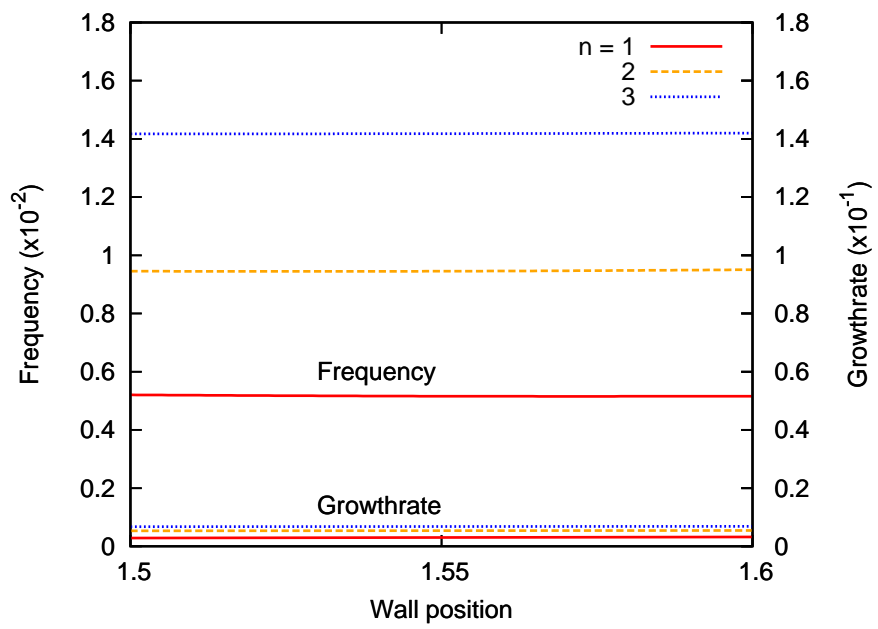


Fig. 12

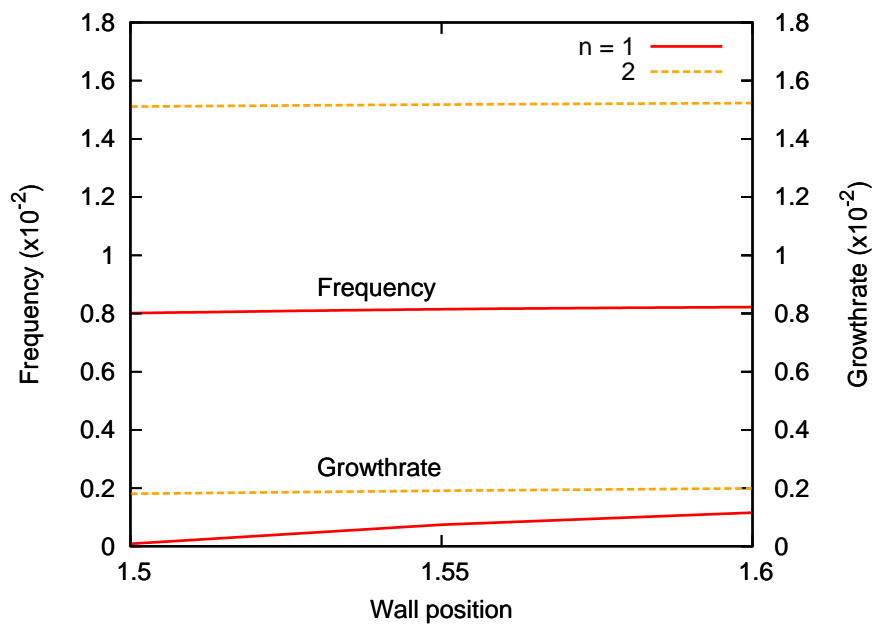


Fig. 13